Journal of Power Sources 195 (2010) 1630–1639

Contents lists available at ScienceDirect

Journal of Power Sources

journal homepage: www.elsevier.com/locate/jpowsour

Effects of anode air bleeding on the performance of CO-poisoned proton-exchange membrane fuel cells

Lung-Yu Sung[a,b], Bing-Joe Hwang[a,c,*], Kan-Lin Hsueh[b,d], Fang-Hei Tsau[b]

[a] Department of Chemical Engineering, National Taiwan University of Science and Technology, Taipei 106, Taiwan
[b] Energy and Environment Research Laboratories, Industrial Technology Research Institute, Hsinchu 310, Taiwan
[c] National Synchrotron Radiation Research Center, Hsinchu, 30076, Taiwan
[d] Department of Energy and Resources, National United University, Miaoli 360, Taiwan

ARTICLE INFO

Article history:
Received 14 August 2009
Received in revised form
23 September 2009
Accepted 30 September 2009
Available online 7 October 2009

Keywords:
Proton-exchange membrane fuel cell
Anode air bleeding
CO poisoning
Reformatted gas

ABSTRACT

In the present work, the dynamic behavior of a PEM fuel cell under CO-poisoning and the effects of air bleeding on the recovery ratio are reported. Pt–Ru catalyst is used as the anode in a single cell and the hydrogen is pre-mixed with 53 ppm of CO as the fuel. The result indicates that even using a CO-tolerant catalyst, CO-poisoning cannot be avoided with the operating conditions in our study. About 80% of the output current is lost within 20 min. Upon anode air bleeding with 5% air, 90% of the current is recovered within 1 min. Higher air bleeding ratio only results in minor improvement of the cell performance. We have developed a transient model to estimate the current reduction due to CO-poisoning and to evaluate the amount of air bleeding needed for a given recovery ratio. A long-term durability test has also been conducted using simulated reformatted gas, in which 1% O_2 is injected into the fuel stream. After more than 3000 h, the cell voltage degradation is less than 3%.

1. Introduction

The proton-exchange membrane (PEM) fuel cell has superior performance over other types of fuel cells. Its applicability in stationary power generation, mobile power for electrical vehicles, and portable power for notebook PCs and other electronic devices has been successfully demonstrated. The PEMFC uses either hydrogen or hydrocarbons as the fuel. Maximum power density can be achieved by using hydrogen as the fuel. However, it has many barriers and issues that need to be overcome, such as storage, delivery, international standards, safety regulations, etc. At present, the application of hydrogen-feed PEMFCs remains limited.

The PEMFC can also use hydrocarbon fuels, including natural gas, methanol, liquefied petroleum gas (LPG), diesel, gasoline, etc. Storage and transportation technologies, safety regulations, and standards for these chemicals are well established since they are used in our daily lives. A reformer is used in the PEMFC power unit to convert hydrocarbons into 35–75% hydrogen-rich gas (so-called reformatted gas). The reformatted gas is then fed into the fuel cell stack for power generation. PEMFC applications in the commercialization stage include the combined heat and power (CHP) unit. The CHP uses the hydrocarbon fuels mentioned above. It produces sufficient electricity (1–5 kW) and heat for a single family house.

During the conversion of hydrocarbon fuels into hydrogen-rich gas, a small amount of carbon monoxide (CO) is produced. Even a trace amount of CO (ppm level) in the anode fuel stream has a detrimental effect on the PEMFC output power. Most PEMFCs use platinum (Pt) as the electrode catalyst. CO molecules have a strong tendency to adsorb at the active sites of the Pt catalyst, which significantly reduces its catalytic activity and hence the output power of the fuel cell. In the long-term, it also causes electrode degradation. This is commonly recognized as CO poisoning.

Overcoming the CO-poisoning problem or enhancing the CO tolerance levels are very important technical challenges for PEMFCs using reformatted gas. Many authors have reported their findings in the literature and have proposed possible solutions [1–13]. At present, a water gas shift reactor (WGS) followed by a preferential oxidation reactor (PROX) is used to reduce the amount of CO in the hydrogen-rich gas from a few percent to ppm [1–3]. A CO-poisoned electrode can be regenerated by periodic pulsed oxidation [4]. A fuel cell operating at high temperature and pressure has been found to have better CO tolerance than one operating at low temperature and pressure [5]. The CO-poisoning effect becomes less severe as the anode flow rate is decreased [6]. Both Pt–Ru and Pt–Sn catalysts show higher CO tolerance levels than Pt catalyst alone [7,8]. A composite (two-layer) anode showed better CO tol-

* Corresponding author at: Department of Chemical Engineering, National Taiwan University of Science and Technology, Taipei 106, Taiwan.
Tel.: +886 2 27376624; fax: +886 2 27376644.
E-mail address: bjh@mail.ntust.edu.tw (B.-J. Hwang).

0378-7753/$ – see front matter © 2009 Elsevier B.V. All rights reserved.
doi:10.1016/j.jpowsour.2009.09.062

Nomenclature

b_c	ratio between reverse/forward rate constant of CO adsorption/desorption (atm)
b_h	ratio between reverse/forward rate constant of H_2 adsorption/desorption (atm)
b_n	ratio between reverse/forward rate constant of N_2 adsorption/desorption (atm)
E_{cell}	cell output voltage (V)
E_o	open-circuit voltage (V)
F	Faraday constant (96,485 C mol^{-1})
i	current density on the electrode (mA cm^{-2})
i_{init}	initial cell output current density before CO is introduced (mA cm^{-2})
i_{oc}	exchange current density of the cathode reduction (mA cm^{-2})
i_{ss}	steady-state cell current density without air bleeding (mA cm^{-2})
i_{ssa}	steady-state cell current density with air bleeding (mA cm^{-2})
k_c	forward rate constant of CO adsorption/desorption (mA cm^{-2} atm^{-1})
k_{eh}	forward rate constant of H_2 electro-oxidation (mA cm^{-2} atm^{-1})
k_h	forward rate constant of H_2 adsorption/desorption (mA cm^{-2} atm^{-1})
k_o	forward rate constant of O_2 adsorption/desorption (mA cm^{-2} atm^{-1})
k_{oc}	forward rate constant of CO–O oxidation (mA cm^{-2} atm^{-1})
k_{oh}	forward rate constant of H–O oxidation (mA cm^{-2} atm^{-1})
k_n	forward rate constant of N_2 adsorption/desorption (mA cm^{-2} atm^{-1})
P	overall gas pressure (atm)
R	universal gas constant (8.314 J mol^{-1} K^{-1})
R_{ohmic}	internal resistance of fuel cell (mΩ cm^2)
r_{air}	recovery ratio of cell output current density (%)
T	temperature (K)
t	time (s)
x_c	molar fraction of CO
x_h	molar fraction of H_2
x_n	molar fraction of N_2
x_o	molar fraction of O_2

Greek letters

α_a	charge-transfer coefficient of hydrogen electro-oxidation
α_c	charge-transfer coefficient of oxygen electro-reduction
η_a	overpotential of the anode (V)
η_c	overpotential of the cathode (V)
η_Ω	overpotential due to internal resistance (V)
θ_c	fractional coverage of CO
θ_h	fractional coverage of H_2
θ_n	fractional coverage of N_2
θ_o	fractional coverage of O_2
ρ	molar area density of catalyst sites in terms of electric charge (mC cm^{-2})

erance than a traditional electrode [9]. Addition of liquid hydrogen peroxide (H_2O_2) to the anode fuel stream may also enhance the CO tolerance level [10]. Injection of a small amount of air into the anode fuel stream can reduce the CO level [11,12]. The oxygen in air oxidizes CO to form CO_2. This method is commonly known as air bleeding. Air bleeding is not a perfect solution for CO poisoning. It causes cell degradation in the long-term. Inaba et al. [13] found that the oxygen on the anode side not only reacts with CO, but is also reduced to hydrogen peroxide (H_2O_2). The H_2O_2 attacks polymers inside the electrode and the proton-exchange membrane. This causes degradation of cell performance. The output power of a CO-poisoned fuel cell can be recovered by removing CO from reformatted gas, anode air bleeding, using CO-tolerant catalysts (Pt–Ru or Pt–Sn), and/or by employing alternative operating conditions. Among these approaches, anode air bleeding is the most effective method since it is simple, efficient, and inexpensive. Although the benefits of air bleeding for the performance of CO-poisoned PEM fuel cells are well known, the effects on long-term durability and recovery ratio of cell current of different concentrations of air bleeding are not clear.

Hence, the objective of the present work has been to investigate the dynamic response of CO poisoning and the recovery ratio of cell performance at different concentrations of air bleeding. The chosen anode fuel stream has been hydrogen containing 53 ppm CO. We have measured polarization curves for a single cell at various levels of air bleeding. The dynamic responses of output current at constant cell voltage with various levels of air bleeding have been measured. A mathematical model has also been developed to calculate cell performance at various CO levels and the recovery ratios of cell current density with various amounts of air bleeding. In addition, a 3000 h long-term durability test on a single cell under anode air bleeding conditions has been carried out. For this test, a simulated reformatted gas (SRG) was used and the degradation rate was measured.

2. Theoretical model

The mechanism of CO poisoning and the method for enhancing the CO-tolerance level have also been studied theoretically. In general, three types of CO-poisoning model have been developed, namely steady state, transient, and one-dimensional transient models. Springer et al. [14] proposed an electrode kinetics model and calculated the steady-state polarization curves under different CO-poisoning conditions. Based on simplified electrode kinetics, a dynamic model was devised whereby the fuel cell output current could be calculated as a function of time after the introduction of CO into the anode fuel stream [15,16]. Many one-dimensional dynamic CO-poisoning models have also been proposed [17–21]. The concentrations of various species and other properties were calculated as a function of time across the electrodes when CO was introduced to the anode or air bleeding was applied. The transient behavior of CO along the flow direction in a single flow channel was also calculated [22]. Fuel cell response under a pulsed voltage treatment to strip adsorbed CO was calculated by Farrell et al. [23]. These dynamic models provide the dynamic response of CO concentration (x_c) and other variables throughout a porous anode. The CO adsorption competes with hydrogen adsorption at the catalyst sites. Once the CO is adsorbed at the active sites, it can only be slowly desorbed. In air bleeding, oxygen reacts with adsorbed CO to form CO_2, and as a result the CO is removed at a much faster rate than in the absence of oxygen. Modeling results [14–23] indicate that the cell output current is very sensitive to trace amounts of CO; it decreases as x_c is increased. The time required for the cell current to reach its steady state is longer for low x_c than for high x_c. The cell current will be recovered once the CO is removed from the anode fuel stream. However, the recovery rate is much slower than that when air is introduced into the fuel stream.

The present model is similar to those proposed by Springer et al. [14], Bhatia and Wang [15], and Zamel and Li [17]. Since operation of CHP with air bleeding condition would be more practical

in real application, modifications of the model proposed in Ref. [17] were made to fit the air bleeding operation condition for consideration of the nitrogen adsorption/desorption on the active site of the catalyst. Mass-transport behavior is neglected and only the electrode reactions are considered. In applying this model, the following assumptions are made:

(a) The effects of the flow channel on the mass-transfer rate are negligible. Species concentrations are uniform throughout the cell.
(b) The diffusion processes of species inside the electrodes are neglected. The species concentrations are uniform throughout the electrode.
(c) Oxygen electro-reduction at the cathode is an irreversible reaction and the Tafel equation is used. Oxygen oxidation and electro-reduction at the anode are neglected.
(d) Hydrogen electrochemical oxidation/reduction on the anode side is a reversible reaction and the Butler–Volmer equation is used. The chemical oxidation of hydrogen with oxygen at the anode is an irreversible reaction but its rate is negligible compared with that of the electrochemical oxidation of hydrogen.
(e) The oxidation of CO at the anode is an irreversible reaction and the electro-oxidation of CO is neglected in our model.

When hydrogen containing a trace amount of CO is introduced, several reactions take place at the anode. The adsorption/desorption and electro-oxidation of hydrogen may be expressed by the Tafel–Volmer mechanism. Here, M represents free catalyst sites and M–H represents a hydrogen atom adsorbed on the catalyst M.

$$\text{hydrogen adsorption/desorption}: H_2 + 2M \Leftrightarrow 2(M\text{–}H) \quad (1)$$

$$\text{hydrogen electrochemical oxidation/reduction}: (M\text{–}H) \Leftrightarrow H^+ + e^- + M \quad (2)$$

The adsorption/desorption and electro-oxidation of CO are expressed by the following reaction pair mechanism.

$$\text{CO adsorption/desorption}: CO + M \Leftrightarrow M\text{–}CO \quad (3)$$

$$\text{CO electro-oxidation}: (M\text{–}CO) + H_2O \rightarrow M + CO_2 + 2H^+ + 2e^- \quad (4)$$

Introducing oxygen or air into the anode fuel stream will reduce the poisoning effect of CO on the anode catalyst layer. The O_2 may react with adsorbed CO to form CO_2 or with adsorbed H atoms to form H_2O. These reactions are described by Eqs. (5)–(7).

$$\text{oxygen adsorption}: O_2 + 2M \rightarrow 2(M\text{–}O) \quad (5)$$

$$\text{CO oxidation}: M\text{–}O + M\text{–}CO \rightarrow 2M + CO_2 \quad (6)$$

$$\text{hydrogen oxidation}: M\text{–}O + 2(M\text{–}H) \rightarrow 3M + H_2O \quad (7)$$

When air is introduced into the anode fuel stream instead of pure oxygen, the adsorption of nitrogen also needs to be considered. Although the nitrogen in air is chemically inert, it adsorbs on the catalyst surface and occupies the catalyst active sites. The adsorption/desorption of N_2 is described by Eq. (8).

$$\text{nitrogen adsorption/desorption}: N_2 + 2M \Leftrightarrow 2(N\text{–}M) \quad (8)$$

The rates of the above equations are dependent on the molar fractions of H_2 (x_h), CO (x_c), O_2 (x_o), and N_2 (x_n); the surface fractional coverages of H_2 (θ_h), CO (θ_c), O_2 (θ_o), and N_2 (θ_n); and the current density on the electrode (i). Eqs. (9)–(12) represent the species balances of H_2 (θ_h), CO (θ_c), O_2 (θ_o), and N_2 (θ_n), respectively. Here, k_h and b_h are the rate constants of H_2 adsorption/desorption; k_c and b_c are the rate constants of CO adsorption/desorption; k_{oc} is the rate constant of CO–O oxidation; k_o is the rate constant of O_2 adsorption; k_{oh} is the rate constant of H–O oxidation; and k_n and b_n are the rate constants of N_2 adsorption/desorption. Thus, k_h, k_c, k_o, k_{oc}, k_{oh}, and k_n are the forward rate constants, while b_h, b_c, and b_n are the ratios of the rate constants of the reverse and forward reactions. P is the overall gas pressure and ρ is the molar area density of catalyst sites in terms of electric charge.

$$\rho\frac{d\theta_h}{dt} = k_h x_h P(1-\theta_h-\theta_c-\theta_o-\theta_n) - b_h k_h \theta_h - i \quad (9)$$

$$\rho\frac{d\theta_c}{dt} = k_c x_c P(1-\theta_h-\theta_c-\theta_o-\theta_n) - b_c k_c \theta_c - k_{oc}\theta_o\theta_c \quad (10)$$

$$\rho\frac{d\theta_o}{dt} = k_o x_o P(1-\theta_h-\theta_c-\theta_o-\theta_n) - k_{oh}\theta_h^2\theta_o - k_{oc}\theta_c\theta_o \quad (11)$$

$$\rho\frac{d\theta_n}{dt} = k_n x_n P(1-\theta_h-\theta_c-\theta_o-\theta_n) - b_n k_n \theta_n^2 \quad (12)$$

The cell output voltage (E_{cell}) represents the balance of the open-circuit voltage (E_o), the overpotential of the anode (η_a), the overpotential of the cathode (η_c), and the overpotential due to internal resistance (η_Ω). These may be calculated by the Eqs. (13)–(16). The hydrogen electro-oxidation rate is described by the Butler–Volmer equation with the oxidation and reduction transfer coefficients being equal. As mentioned above, the electro-oxidation of CO is neglected in our model. Here, i_{oc} is the exchange current density of the cathode reduction, R_{ohmic} is the internal resistance of the cell, and R, T, F, and α are the universal gas constant, the temperature, the Faraday constant, and the charge-transfer coefficient, respectively; k_{eh} is the rate constant of the hydrogen electro-oxidation reaction.

$$E_{cell} = E_o - \eta_a - \eta_c - \eta_\Omega \quad (13)$$

$$\eta_c = \frac{RT}{\alpha_c F}\ln\left(\frac{i}{i_{oc}}\right) \quad (14)$$

$$\eta_a = \frac{RT}{\alpha_a F}\sinh^{-1}\left(\frac{i}{2k_{eh}\theta_h}\right) \quad (15)$$

$$\eta_\Omega = iR_{ohmic} \quad (16)$$

The numerical solution is obtained by means of a program written in Fortran language. The procedure is given in the following. A finite difference method is used to solve the differential Eqs. (9)–(12). The parameters in the Eqs. (14)–(16), α_c, α_a, i_{oc}, k_{eh}, and R_{ohmic}, are calculated from the best fitting of the polarization curves (Figs. 5 and 6). The values of all of the "k" and "b" parameters in the Eqs. (9)–(12) are calculated from the best fitting of the current density response curves. Surface fractional coverages (θ_h, θ_c, θ_o, θ_n) are calculated as a function of time from the Eqs. (9)–(12). The value of θ_h is then used to calculate the output current density (i) under conditions of constant cell voltage (E_{cell}) from the Eqs. (13)–(16). The calculated current density is then used to solve the Eqs. (9)–(12). Several iterations are required before the Eqs. (9)–(16) reach convergence. These variables (θ_h, θ_c, θ_o, θ_n, and i) are solved as a function of time (t).

3. Experimental

A single cell was used for all of the experiments reported herein. The specifications of this testing cell are listed in Table 1. The membrane electrode assembly (MEA) used Gore PRIMEA® 5621 with an electrode active area of 25 cm^2 (5 cm × 5 cm). Pure hydrogen and hydrogen pre-mixed with 53 ppm CO were used as fuels for the anode in our experiments. Air and oxygen were used as cathode feeds. Nitrogen was used for purging the system. Fig. 1 shows the piping and electrical connections of the experimental set-up. Gas flow rates were controlled by the mass flow controller (Protec

Table 1
Component items and specifications of test cell.

Component items	Specifications
MEA (CCM)	Gore PRIMEA® 5621
Membrane	35 μm/composite membrane
Active area	25 cm^2
Loading of catalyst	0.45 mg cm^{-2} Pt–Ru (anode) 0.6 mg cm^{-2} Pt (cathode)
GDL (carbon cloth)	400 μm/CARBEL® CL
Flow field plate (graphite)	POCO
Configuration of flow channels	65 cm/serpentine
No. of flow channels	Two
Flow channel width/depth/interval	1 mm/1 mm/1 mm

Table 2
Test conditions of PEM fuel cell.

Items	Test conditions
Conc. of carbon monoxide	53 ppm
Conc. of anode air bleeding	2%, 3%, 4%, 5%, 8%, 10%, 15%, 20% air
Cell operation temp.	65 °C
Cell operation voltage	0.6 V
H_2/O_2/air stoich. ratio	1.5 X/2.0 X/2.0 X
H_2/O_2/air humidification temp.	80 °C/70 °C/70 °C
H_2, O_2, air pressure	Ambient pressure
Simulated reformatted gas (SRG)	45% H_2, 17% CO_2, 3% CH_4, 25 ppm CO, 1% O_2, N_2 (balance gas)

Instruments, Inc., model PC-540). All gases were humidified prior to entering the cell by bubbling them through a water tank. Their humidity was controlled by adjusting the temperature of the water tank. Water in the exhaust gases was separated by a gas/liquid separator. During the air bleeding experiment, air was mixed into the anode fuel stream. The amount of air bleeding was adjusted by controlling the air flow rate. The cell was heated by means of two heating rods inserted into graphite plates on either side of the testing cell. Its temperature was regulated by a temperature controller (YSC, model GX-36). Cell output voltage and current were measured and controlled by an electronic load (Hewlett-Packard Co., model 6060B).

In order for the cell to reach a steady state quickly, a series of activation steps was applied after its assembly. During the cell activation, various current densities ranging from 100 to 600 mA cm^{-2} were applied for 20–30 h. Once the cell reached a steady state, experiments were started under the testing conditions listed in Table 2.

4. Results and discussion

When the CO-contaminated hydrogen was introduced into the anode, the cell performance was not affected at first. This may be attributed to the fact that the diffusion rate of hydrogen is faster than that of CO. However, once the CO had diffused through the gas diffusion layer (GDL) and had reached the catalyst layer, the cell performance quickly diminished. The CO molecules competed with hydrogen molecules for sites on the catalyst surface. The CO was adsorbed on the catalyst surface and hence the catalyst lost its activity.

4.1. Effects of CO in the hydrogen stream on cell performance

Fig. 2 shows the cell current density responses at 0.6 V when the anode fuel stream was changed from pure H_2 to H_2/CO and then from H_2/CO back to pure H_2. Two sets of data were obtained. One set was obtained for a cathode with an oxygen stream and a further set was obtained for a cathode with an air stream. The concentration of CO in the hydrogen was around 53 ppm. At t = 15 min, H_2/CO was introduced into the anode, and as a result the cell output current density sharply decreased to a lower value over 20 min (t = 35 min). For the oxygen stream cathode, the current density decreased by 82%, dropping from 1900 to 340 mA cm^{-2}. The degradation rate of current density was about 78 mA cm^{-2} min^{-1}. For the air feed cathode, the current density decreased by 80%, dropping from 1050 to 220 mA cm^{-2}. The degradation rate was about 42 mA cm^{-2} min^{-1}. Although the CO concentration was only 53 ppm, this contaminant level quickly poisoned the catalyst and thus had a detrimental effect on the cell performance. After 30 min (t = 45 min), the current densities reached steady values of 290 mA cm^{-2} for oxygen and 210 mA cm^{-2} for air, this steady state corresponding to an equilibrium of CO absorption and desorption. The cell output current density gradually increased when the anode feed stream was changed from H_2/CO back to pure H_2 (t = 52 min). The recovery rate was slow, with about 60 min being required for the current density to return to 90% of its original value. This suggests that using Pt–Ru as the anode catalyst does not provide a significant improvement of CO tolerance. However it may be improved to with different operating conditions (higher operating temperature, etc.). In our study, the cell performance could not be completely recovered from the effects of CO poisoning by simply replacing Pt with Pt–Ru at the operating temperature of 65 °C.

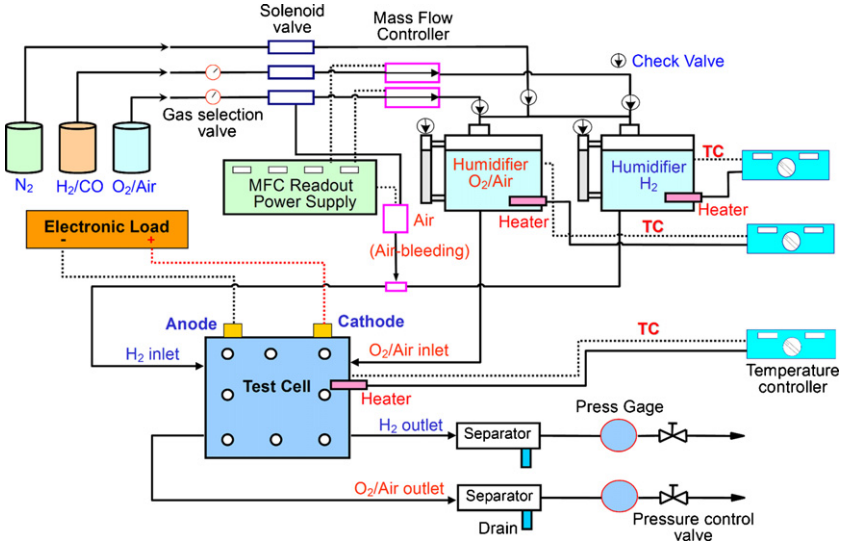

Fig. 1. Piping and electrical connections of the experimental set-up.

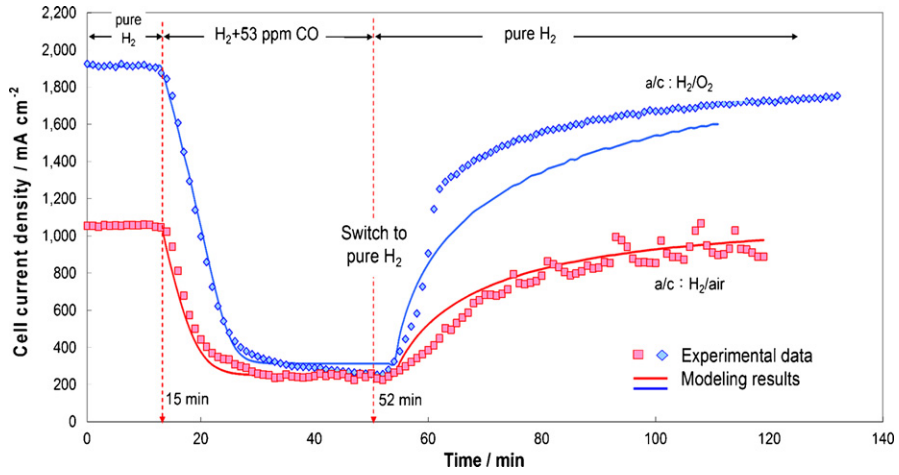

Fig. 2. Effects of CO on output current. This figure plots dynamic response of cell current density versus time. Hydrogen containing 53 ppm CO gas was introduced at $t = 15$ min. Pure hydrogen was introduced at $t = 52$ min. One curve is for the cathode with pure O_2 feed and the other curve is for air feed.

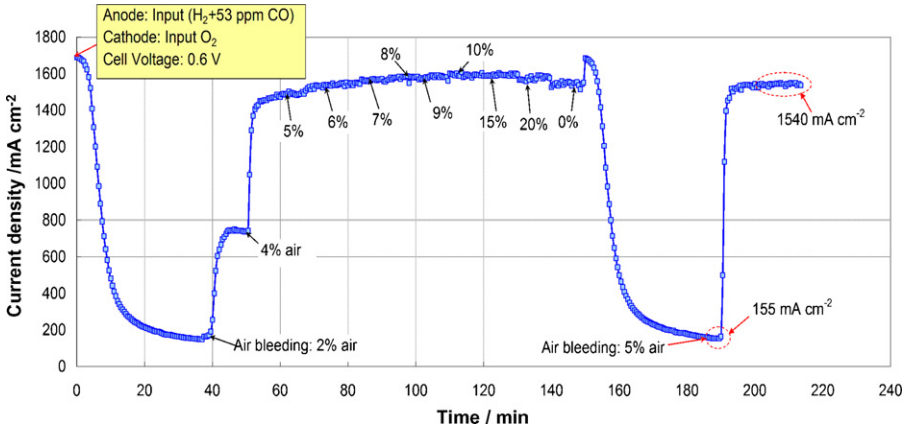

Fig. 3. Effects of air bleeding on the output current density of a CO-poisoned single cell. This figure plots dynamic response of current density at 0.6 V versus time. Hydrogen containing 53 ppm CO gas was introduced at $t = 0$ min. Air at different concentrations was introduced into the anode stream at different times, as indicated in the figure. The cathode fuel stream was pure oxygen.

4.2. Effects of anode air bleeding on the cell performance

Figs. 3 and 4 show the cell output current densities at 0.6 V and various levels of anode air bleeding with O_2-feed and air-feed cathodes, respectively. The hydrogen of the anode feed contained 53 ppm CO and the anode air bleeding levels were varied from 2% to 30% air. As can be seen in Fig. 3, when the anode was fed with H_2/CO, within 35 min the current density decreased from 1690 to 155 mA cm^{-2}. However, the CO-poisoning effect could be relieved by injecting a small amount of air into the anode fuel stream. The current density then quickly increased. This was because the oxygen in the air oxidized the CO adsorbed on the catalyst surface

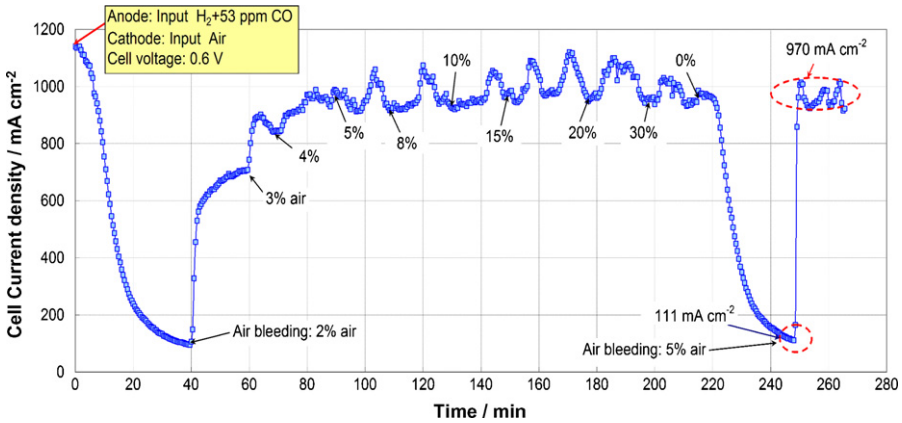

Fig. 4. Effects of air bleeding on the output current density of a CO-poisoned single cell. This figure plots dynamic response of current density at 0.6 V versus time. Hydrogen containing 53 ppm CO gas was introduced at $t = 0$ min. Air at different concentrations was introduced into the anode fuel stream at different times, as indicated in the figure. The cathode fuel stream was air.

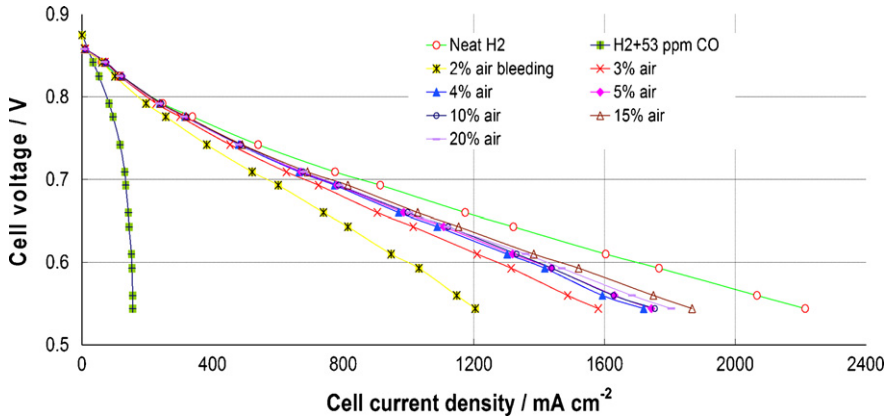

Fig. 5. Plots of cell voltage versus current density under various anode air bleeding conditions. The anode fuel stream consisted of hydrogen containing 53 ppm CO and different concentrations of air. The cathode fuel stream was oxygen.

to CO_2. Once the CO had been removed, the catalyst sites were reactivated and available for hydrogen oxidation once more.

When the anode feed was injected with 2% air, the current density quickly increased from 155 to 740 mA cm^{-2}. The current density increased to 1480 mA cm^{-2} when 4% air was injected into the anode stream and reached 1540 mA cm^{-2} when 5% air was injected. However, the improvement of current density was gradually diminished when the amount of air injected was increased from 5% (about 1% oxygen) to 15% (about 3% oxygen). The current density was seen to decrease when the amount of air injected exceeded 15%. This may be attributed to the fact that injection of a large amount of air into the anode stream dilutes the hydrogen concentration and part of the hydrogen may also be oxidized by the oxygen in the air. Similar results were obtained with the air-feed cathode, as shown in Fig. 4.

4.3. Effects of air bleeding on polarization curves

The polarization curve (current–cell voltage curve) of a testing cell can be obtained in either current-controlled mode or voltage-controlled mode. We used voltage-controlled mode. During the measurements, the cell voltage was scanned from OCV (open-circuit voltage) to a fixed voltage and the current was recorded. Figs. 5 and 6 show the polarization curves obtained with different amounts of anode air bleeding with oxygen-feed and air-feed cathodes, respectively. The testing cell showed superior performance when it was operated with H_2/O_2. The cell performance was significantly degraded when the anode feed contained a trace amount of CO (53 ppm). At a cell voltage of 0.6 V, the output current density was reduced from 1693 to 152 mA cm^{-2} when pure H_2 feed was changed to H_2 containing 53 ppm CO. However, the cell current density could be recovered by injecting a small amount of air into the anode stream, as shown in Fig. 5. The benefits of anode air bleeding were obvious. At a cell voltage of 0.6 V, the current density was recovered from 152 to 1000, 1290, 1390, and 1410 mA cm^{-2} when 2%, 3%, 4%, and 5% air, respectively, was introduced into the anode feed. The amount of recovery was gradually diminished when the air concentration was further increased from 5% to 15%. The current density was seen to decrease when the air concentration exceeded 15% (3% oxygen). Similar results and conclusions were also obtained for the air-feed cathode, as shown in Fig. 6.

4.4. Modeling results

Table 3 lists the parameter values used in the modeling. These values are manually fitted experimental data of voltage–current density curves and current density responses at different levels of air bleeding. The modeling results are compared with the experimental data in Figs. 2 and 7. The curves in these figures are the modeling results. The modeling results are seen to be in reasonable agreement with the experimental data. The current density at a cell voltage of 0.6 V is plotted as a function of time in Fig. 7. The experiment started with pure hydrogen, which was switched to hydrogen containing 53 ppm CO at t = 1.5 min. Different concentrations of air were introduced into the anode fuel stream at t = 27.5 min. The cathode was fed with oxygen during the entire experiment. For clarity, the results of air bleeding at concentrations of 8% and 15% are not included in this figure.

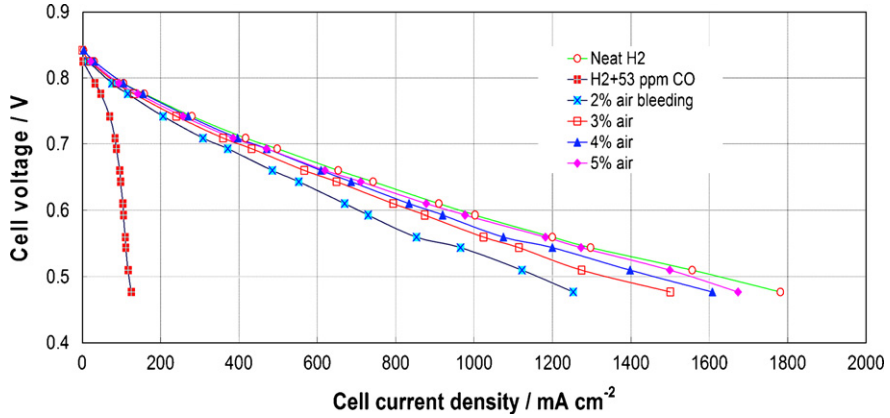

Fig. 6. Plots of cell voltage versus current density under various anode air bleeding conditions. The anode fuel stream consisted of hydrogen containing 53 ppm CO and different concentrations of air. The cathode fuel stream was air.

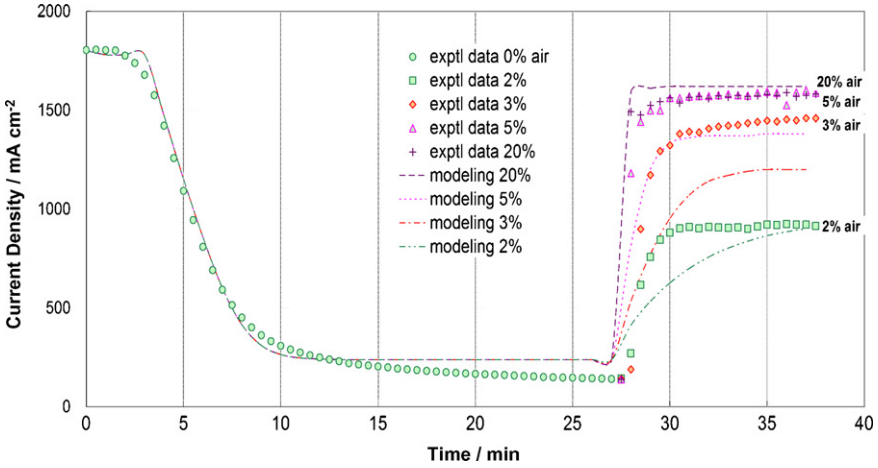

Fig. 7. Comparison between experimental data and the modeling results. The plots show the dynamic response of current density at a cell voltage of 0.6 V versus time for a CO-poisoned cell under different air bleeding conditions (2%, 3%, 5%, 20% air). The anode fuel stream consisted of hydrogen containing 53 ppm of CO. The cathode fuel stream was oxygen.

Table 3
Parameter values used in the modeling.

Parameters	Value
P, atm	1
T, K	338
ρ, mC cm^{-2}	100
E_o, V	1.24
k_{eh}, mA cm^{-2} atm^{-1}	0.54
k_h, mA cm^{-2} atm^{-1}	200
b_h, atm	0.062
k_c, mA cm^{-2} atm^{-1}	300
k_o, mA cm^{-2} atm^{-1}	3.9
k_{oc}, mA cm^{-2} atm^{-1}	100
k_{oh}, mA cm^{-2} atm^{-1}	600
k_n, mA cm^{-2} atm^{-1}	0.001
b_n, atm	0.5
α_a, α_c	0.36
R_{ohmic}, mΩ cm^2	100
i_{oc}, mA cm^{-2}	1.5×10^{-10}
b_c, atm	1.0×10^{-7}

Using the parameter values listed in Table 3, the effects of CO concentration on the dynamic response of cell output current density are plotted in Fig. 8. The current density decreased sharply when an H_2 feed stream containing CO was introduced, eventually reaching a steady-state current density (i_{ss}). The time required to reach a steady state (t_{ss}) was shorter for a high CO concentration than for a low CO concentration. For example, t_{ss} was greater than 36 min at a CO level of 10 ppm but less than 8 min at a CO level of 100 ppm. The steady-state current density (i_{ss}) was also influenced by the CO concentration. The i_{ss} was lower at a high CO concentration than at a low CO concentration. The i_{ss} decreased from 1780 to 780 mA cm^{-2} when 10 ppm CO was introduced. However, the i_{ss} remained at 140 mA cm^{-2} when the CO concentration was increased from 90 to 100 ppm. Thus, i_{ss} is more sensitive to changes of CO concentration at low levels of CO.

The steady-state current density i_{ss} is plotted as a function of air bleeding concentration for different CO concentrations in Fig. 9. In the low air bleeding region (0–4%), it can be seen that i_{ss} significantly increased as the air bleeding concentration was increased. In the high air bleeding region (>6%), only a minor improvement of i_{ss} can be seen as the air bleeding concentration was increased. This suggests that air bleeding at a low air concentration is more effective than that at a high air concentration. At a high air concentration, nitrogen may dilute the concentration of hydrogen and part of the hydrogen may also be oxidized by the oxygen in the air.

An alternative view of the effect of air bleeding on the cell output current was obtained by plotting recovery ratio (r_{air}) as a function of air bleeding concentration (Fig. 10). The recovery ratio is defined as:

$$r_{air} = \frac{i_{ssa} - i_{ss}}{i_{init} - i_{ss}} \quad (17)$$

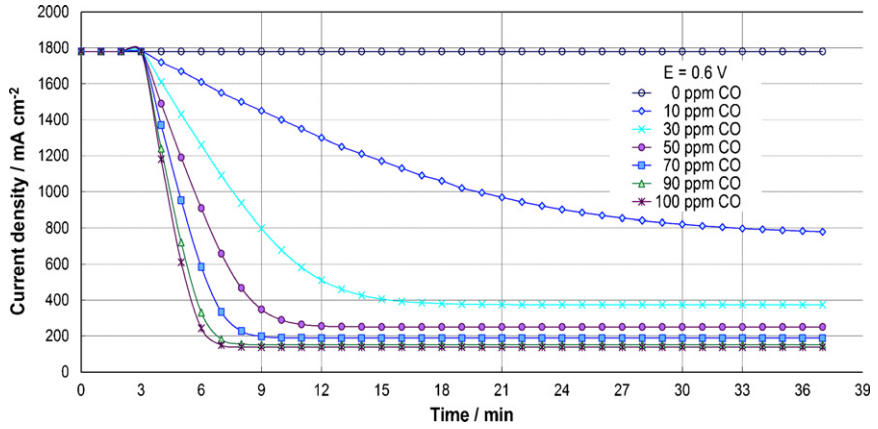

Fig. 8. Dynamic responses of current density at 0.6 V after introducing hydrogen containing different levels of CO (from 0 to 100 ppm) at t = 3 min. The cathode fuel stream was oxygen.

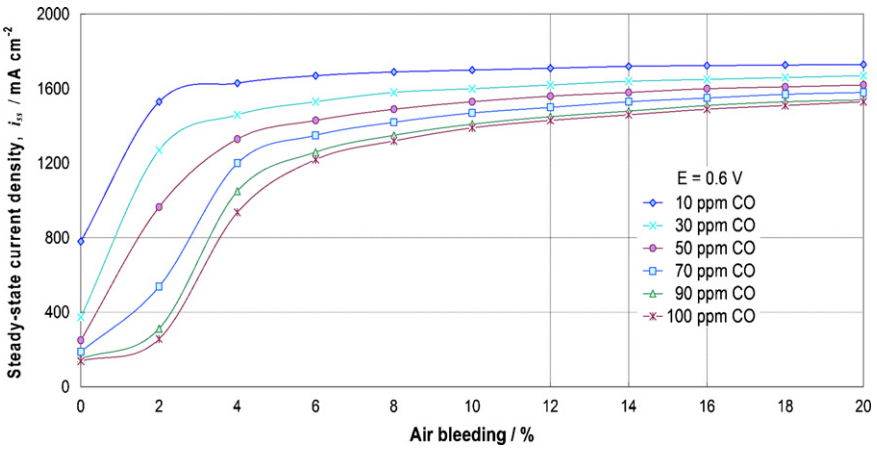

Fig. 9. Effects of air bleeding levels on the steady-state current density, i_{ss}, at 0.6 V. Calculation conditions started with pure hydrogen, then hydrogen containing different levels of CO (from 0 to 100 ppm) was introduced at t = 1.5 min and air was injected into the anode fuel stream at 27.5 min. The cathode fuel stream was oxygen.

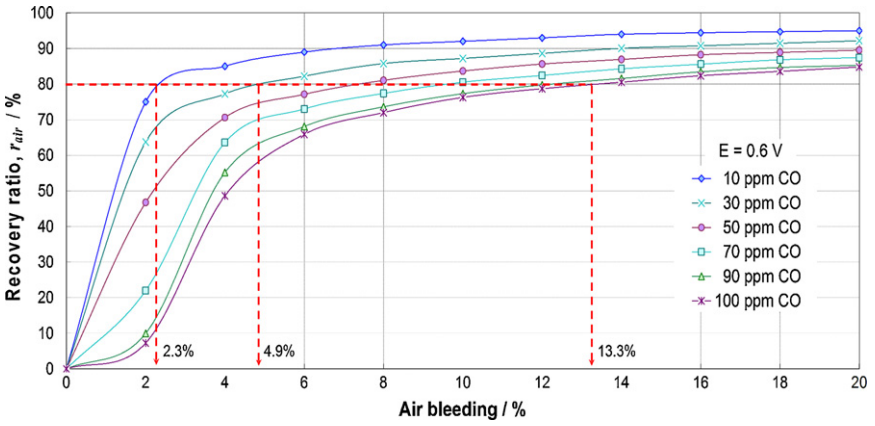

Fig. 10. Effects of air bleeding level on the recovery ratio of current density, r_{air}, at 0.6 V. Calculation conditions started with pure hydrogen, then hydrogen containing different levels of CO (from 0 to 100 ppm) was introduced at t = 1.5 min and air was injected into the anode stream at 27.5 min. The cathode fuel stream was oxygen.

where i_{init} is the initial cell output current density before CO is introduced, i_{ss} is the steady-state current density without air bleeding (i.e., at an air concentration in the anode feed of zero), and i_{ssa} is the steady-state current density with air bleeding. Fig. 10 shows the recovery ratio curves obtained at a cell voltage of 0.6 V. At low CO concentration (10 ppm), the recovery ratio reached 90% with 6.7% air bleeding. At high CO concentration (100 ppm), it proved almost impossible to reach a 90% recovery ratio. As is evident from Fig. 10, such a plot can be used to estimate the amount of air bleeding needed in order to maintain a constant recovery ratio. For instance, to maintain the recovery ratio at 80%, different amounts of air bleeding are needed for various CO levels. The amount of

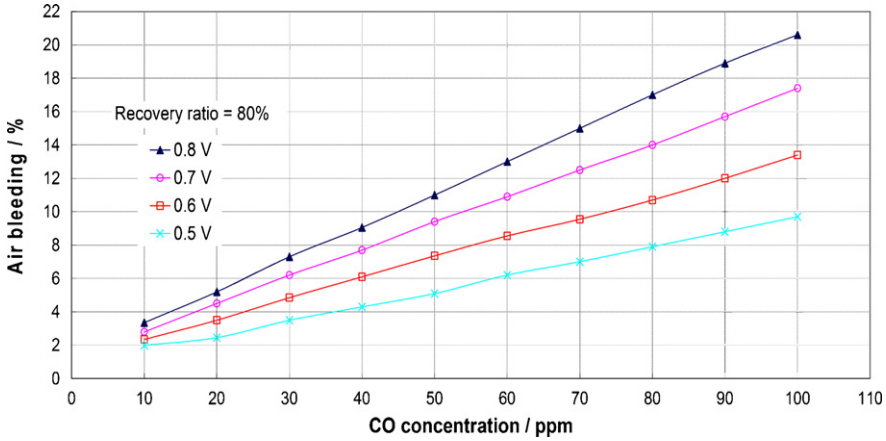

Fig. 11. Plots of air bleeding needed to reach 80% recovery ratio versus CO concentration at different cell output voltages. The calculation conditions were the same as in Fig. 10.

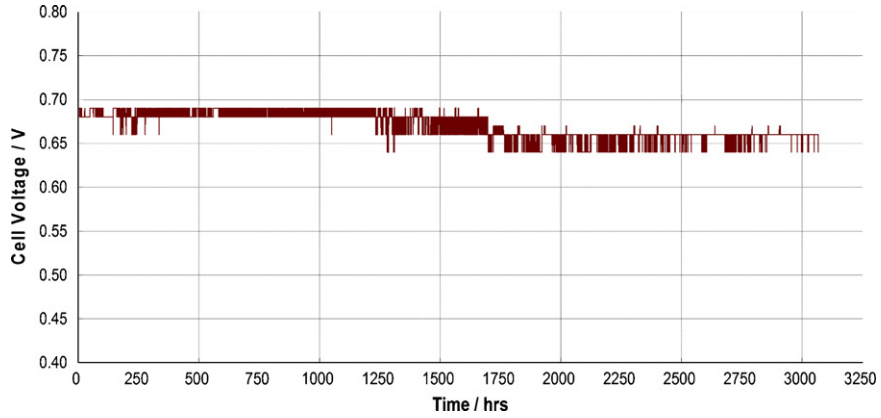

Fig. 12. Long-term durability test of the PEMFC. The test was conducted at a constant current density of 300 mA cm^{-2}. The anode used simulated reformatted gas (SRG) with a composition of 45% H_2, 17% CO_2, 3% CH_4, 25 ppm CO, 1% O_2, and 34% N_2. The cathode used air. The air bleeding level was 1% O_2 (~5% air).

air bleeding needed can be read from Fig. 10. For a recovery ratio of 80%, the amounts of air bleeding needed are 2.3%, 4.9%, and 13.3% at 10 ppm, 30 ppm, and 100 ppm CO, respectively. For practical purposes, the amount of air bleeding needed to reach 80% recovery ratio is plotted as a function of CO concentration in Fig. 11. At constant cell voltage, the amount of air bleeding needed to reach 80% recovery ratio is linearly proportional to the CO concentration. At a given CO concentration, the amount of air bleeding needed to reach 80% recovery ratio is larger at higher cell voltages. For instance, at 30 ppm CO, the amount of air bleeding needed increased from 3.5% to 7.3% when the cell voltage was increased from 0.5 to 0.8 V.

4.5. Effects of air bleeding on the long-term durability of a PEMFC

From the above experimental results, it was concluded that 5% air bleeding was the optimal level with 53 ppm CO in the anode fuel. Each of the aforementioned experiments was carried out within a few hours. The long-term stability of the single cell under air bleeding conditions was unknown. To verify the stability of the single cell under air bleeding, a long-term test was subsequently performed.

The hydrogen concentration in reformatted gas is much lower compared to pure hydrogen and this anode feed contains other gases such as CO_2, CH_4, H_2O, and trace amounts of CO. These gases affect the cell performance and the stability of the key components. Therefore, a long-term durability test is very important for a fuel cell power system with reformatted gas as the input. In assessing the durability of the single cell with air bleeding, as the anode inlet gas we used simulated reformatted gas (SRG) and 1% oxygen, which is equivalent to 5% air.

Fig. 12 shows the durability testing result of a single cell (25 cm^2) at constant current density (300 mA cm^{-2}) over 3000 h. SRG was fed to the anode. The composition of this SRG was 45% H_2, 17% CO_2, 3% CH_4, 25 ppm CO, and 1% O_2, with the balance being N_2. Air was fed to the cathode. The open-circuit voltage (OCV) of the cell was around 0.94 V. At a current density of 300 mA cm^{-2}, the initial cell output voltage was 0.69 V and this was maintained in the range between 0.69 and 0.64 V. The voltage decay rate was small (about 3%). This suggested that the catalyst was not seriously poisoned by the CO under the air bleeding conditions. Injection of a small amount of oxygen (air bleeding) is an effective method for reducing CO poisoning and thereby extending fuel cell operating duration.

5. Conclusions

A single cell with anode fuel containing 53 ppm CO has been used to examine the effects of air bleeding on the cell performance. Our experimental results suggest that even CO-tolerant Pt–Ru catalyst was used as the anode under our operating conditions, about 80% of the output current was lost within 20 min. Nevertheless, with air bleeding with 5% air (~1% O_2) at the anode side, 90% of the current was recovered within 1 min. A transient model has been used to model the dynamic responses of output current under conditions of CO poisoning and with air bleeding. Reasonable agreement between the experimental data and modeling results has been obtained. This model can be used to estimate the degree of current reduction due to different levels of CO poisoning and to evaluate the amount of air bleeding needed for a given recovery ratio of output current density. To verify the stability of a cell under application of the air bleeding technique, a long-term durability test has been conducted using simulated reformatted gas (SRG, containing 45% H_2, 17% CO_2, 3% CH_4, and 25 ppm CO). During the entire testing period, 5% air (~1% O_2) was injected into the anode fuel stream. The cell voltage degradation was less than 3%, or 0.64×10^{-5} V h^{-1}, after testing for more than 3000 h.

Acknowledgements

The authors appreciate for the financial support from the Bureau of Energy of the Ministry of Economical Affairs (MOEA), the National Science Council (NSC), and the National Taiwan University of Science and Technology, Taiwan. Experimental work was carried out at the Fuel Cell Laboratory of EEL/ITRI (Energy and Environmental Laboratories/Industrial Technology Research Institute).

References

[1] T.V. Choudhary, D.W. Goodman, Catal. Today 77 (2002) 65–78.
[2] V. Galvita, K. Sundmacher, Chem. Eng. J. 134 (2007) 168–174.
[3] P.K. Cheekatamarla, W.S. Epling, A.M. Lane, J. Power Sources 147 (2005) 178–183.
[4] W.A. Adams, J. Blair, K.R. Bullock, C.L. Gardner, J. Power Sources 145 (2005) 55–61.
[5] M. Murthy, M. Esayian, W.-k. Lee, J.W. Van Zee, J. Electrochem. Soc. 150 (2003) 29–34.
[6] J. Zhang, T. Thampan, R. Datta, J. Electrochem. Soc. 149 (2002) 765–772.
[7] S.J. Lee, S. Mukerjee, E.A. Ticianelli, J. McBreen, Electrochim. Acta 44 (1999) 3283–3293.
[8] Z. Qi, A. Kaufman, J. Power Sources 113 (2003) 115–123.
[9] H. Yu, Z. Hou, B. Yi, Z. Lin, J. Power Sources 105 (2002) 52–57.
[10] J. Divisek, H.F. Oetjen, V. Peinecke, V.M. Schmidt, U. Stimming, Electrochim. Acta 43 (1998) 3811–3815.
[11] S. Gottesfeld, J. Pafford, J. Electrochem. Soc. 135 (1988) 2651–2652.
[12] W. Shi, M. Hou, Z. Shao, J. Hu, Z. Hou, P. Ming, B. Yi, J. Power Sources 174 (2007) 164–169.
[13] M. Inaba, M. Sugishita, J. Wada, K. Matsuzawa, H. Yamada, A. Tasaka, J. Power Sources 178 (2008) 699–705.

[14] T.E. Springer, T. Rockward, T.A. Zawodzinski, S. Gottesfeld, J. Electrochem. Soc. 148 (2001) A11–A23.
[15] K.K. Bhatia, C.Y. Wang, Electrochim. Acta 49 (2004) 2333–2341.
[16] J.J. Baschuk, X. Li, Int. J. Energy Res. 27 (2003) 1095–1116.
[17] N. Zamel, X. Li, Int. J. Hydrogen Energy 33 (2008) 1335–1344.
[18] H.S. Chu, C.P. Wang, W.C. Liao, W.M. Yan, J. Power Sources 159 (2006) 1071–1077.
[19] C.P. Wang, H.S. Chu, J. Power Sources 159 (2006) 1025–1033.
[20] C.P. Wang, H.S. Chu, Y.Y. Yan, K.L. Hsueh, J. Power Sources 170 (2007) 235–241.
[21] S.H. Chan, S.K. Goh, S.P. Jiang, Electrochim. Acta 48 (2003) 1905–1919.
[22] D.J.L. Brett, P. Aguiar, N.P. Brandon, A.R. Kucernak, Int. J. Hydrogen Energy 32 (2007) 863–871.
[23] C.G. Farrell, C.L. Gardner, M. Ternan, J. Power Sources 171 (2007) 282–293.